



Patrick Simmons, Scott Bryson

Position Sensing

## ABSTRACT

Joystick and Lever functions are commonly used as an input control for various applications which include game controllers, heavy machinery, and automotive eShifters and steering column stalks. In each case, the joystick or lever is allowed one or two axes of rotation. Strategic placement of magnets and Hall-effect sensors within these systems provide a useful format to eliminate contact based components which wear out over time.

This document demonstrates implementations of both a video game controller thumb toggle joystick using and a retro-fitting of a production automotive turn indicator stalk found within a steering column control module. In both configurations, 3D linear Hall-effect sensors are used to capture magnetic field data. Setup and testing methods are detailed along with an analysis of mechanical error sources which can influence the measurement quality.

---

## Table of Contents

<b>1 Introduction</b> .....	2
<b>2 Joystick Design</b> .....	3
2.1 Establishing Form Factor.....	3
2.2 Magnet Sensor Placement.....	5
2.3 Design Calculations.....	8
2.4 Post Processing.....	11
2.5 Prototyping and Bench Testing.....	13
2.6 Error Sources.....	15
<b>3 Lever Design</b> .....	19
3.1 Establishing a Form Factor.....	19
3.2 Magnet Sensor Placement.....	21
3.3 Design Calculations.....	22
3.4 Prototyping and Bench Testing.....	24
3.5 Error Sources.....	26
<b>4 Summary</b> .....	27
<b>5 References</b> .....	27
<b>6 Revision History</b> .....	27

## Trademarks

All trademarks are the property of their respective owners.

## 1 Introduction

This document provides a high-level view of joysticks and levers while showing how such controls can be constructed with Hall-effect sensors. In conjunction with the high-level discussion, design examples are presented. [Figure 1-1](#) summarizes the design flow for the presented design examples.

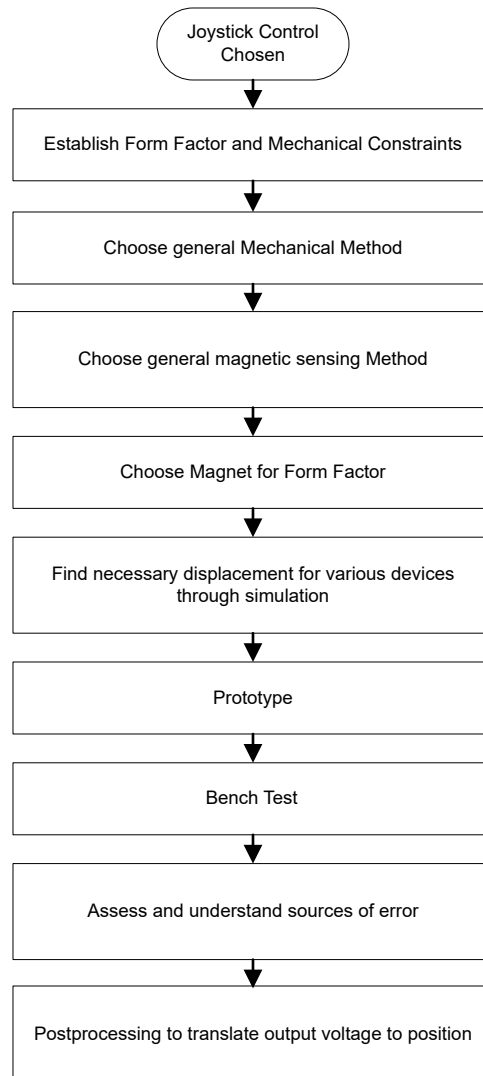


**Figure 1-1. Development Flow**

## 2 Joystick Design

### 2.1 Establishing Form Factor

The mechanical form factor provides the bounds for the system implementation and dictates what size magnet or grade of magnet needs to be considered for the construction of your joystick or lever. Typically, Hall-effect sensors measure the magnetic field emanating from a permanent magnet. Unless the Hall-effect sensor is wired up with something similar to slip ring or is controlled from a local wireless module, the hall-effect sensor is most likely reside in the stationary part of the joystick, while the magnet is in one of the bodies that has some free range of motion. The magnet is some dimension smaller than that body. Consequently, for a subset of joysticks commonly called thumbsticks in gaming controllers, design is limited to a small magnet. Typically, only neodymium magnets are found in such a small form factor and these magnets are stronger, have greater temperature drift, and cost more.

#### 2.1.1 Choosing Mechanical Implementation

Depending on the equipment purpose, the resolution, the features, cost, ease of manufacturing, and the desired user experience, different mechanical methods might be explored. Below are just a few options of what might be considered. Methods 1 and 2 are variations of the ball and socket joint, illustrating that the ball can be in the stationary or mobile body of the joint, depending on whichever seems more suitable for design. Method 3 illustrates an example of a joystick with 2 axes, allowing 2 degrees of motion through 1 stationary body and two mobile bodies.

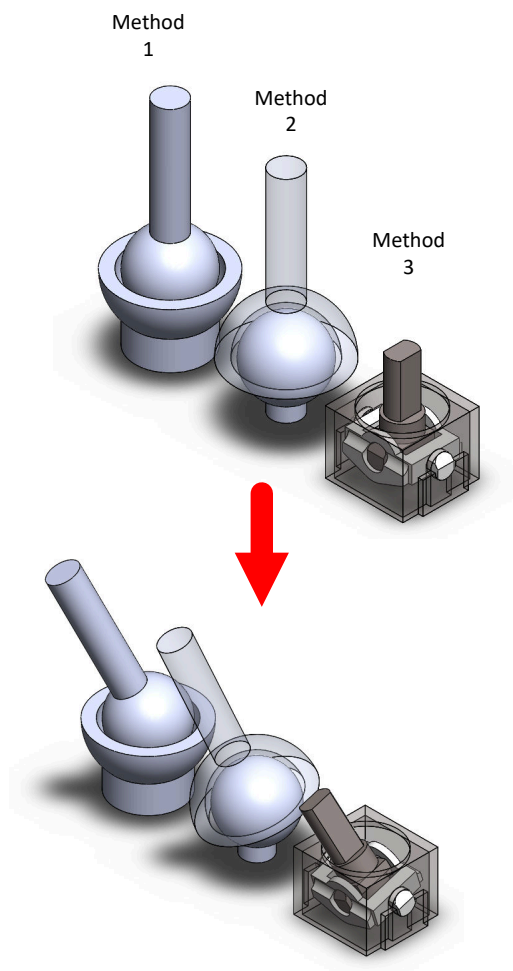


**Figure 2-1. Mechanical Implementations**

### 2.1.2 Choosing Magnetic Implementation

The magnetic implementation corresponds to the type of magnet, the path of motion, and the orientation of the magnet and sensor relative to each other. Figure 2-2 shows a couple possible magnetic implementations per mechanical method introduced in Figure 2-1. Starting from the left, there are two mechanical method 1 options with either a sphere or cylindrical magnet. Then in the middle are two mechanical method 2 options with either an axial ring magnet or a diametric ring magnet. Lastly on the right are two mechanical method 3 options, with one having a central axial ring magnet on the joystick shaft, while the other has two bar magnets that rotate with the axles. Each of these has unique design challenges and may have a unique sensor pairing.

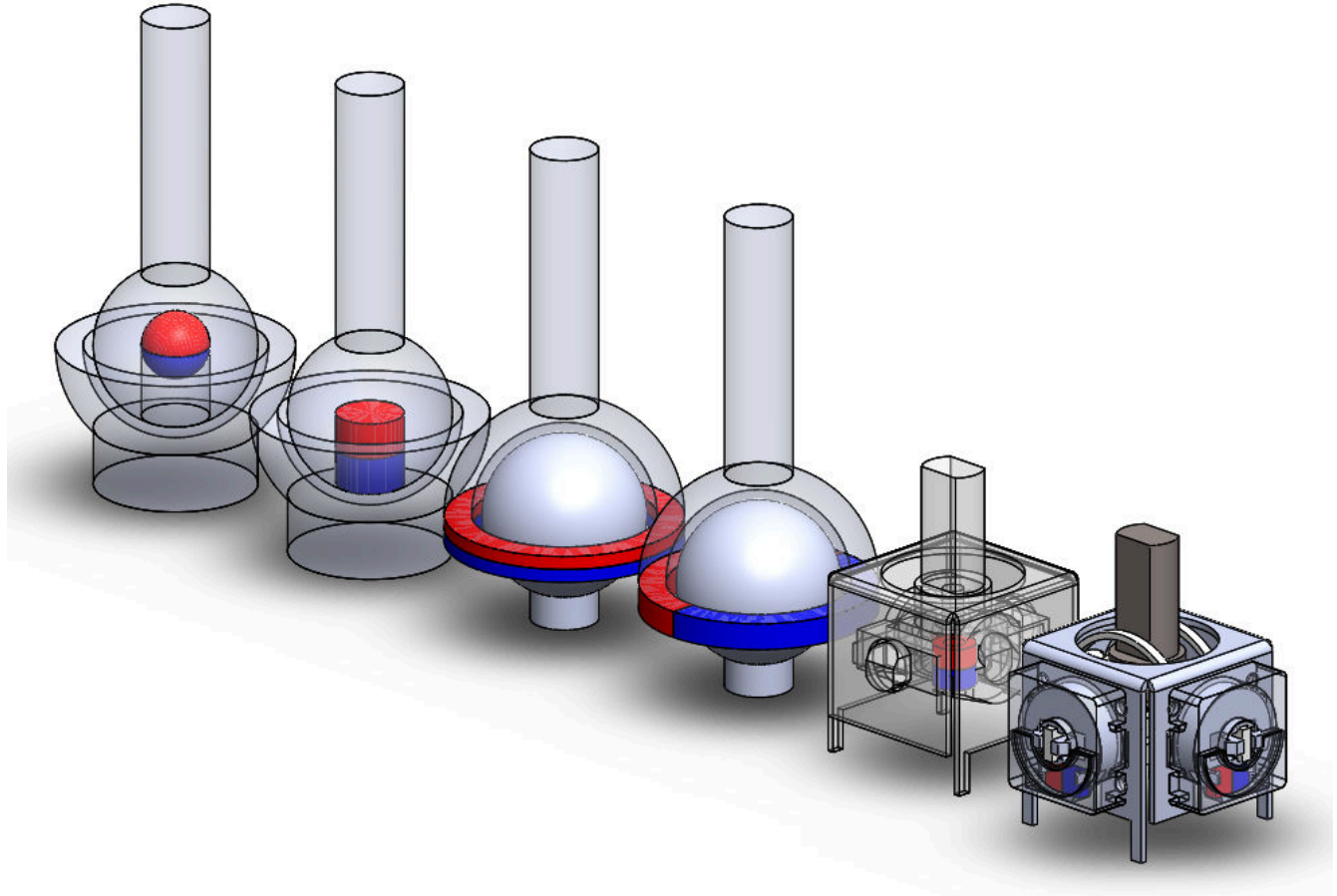


**Figure 2-2. Magnetic Implementations**

## 2.2 Magnet Sensor Placement

The end goal is to map the device output to a distinct mechanical position. As our magnet contained in the moving body is not confined to a single straight path, but rather a rotation, yawing, tilting, or pitching within one or more planes, at least 2 Hall-Elements are needed to avoid spatial aliasing as indicated in Figure 2-3. Figure 2-4 illustrates that with data from perpendicular sensing elements, both a unique joystick pitch value and unique rotation value can be extracted from 2 sensors that by themselves can not distinguish joystick position.

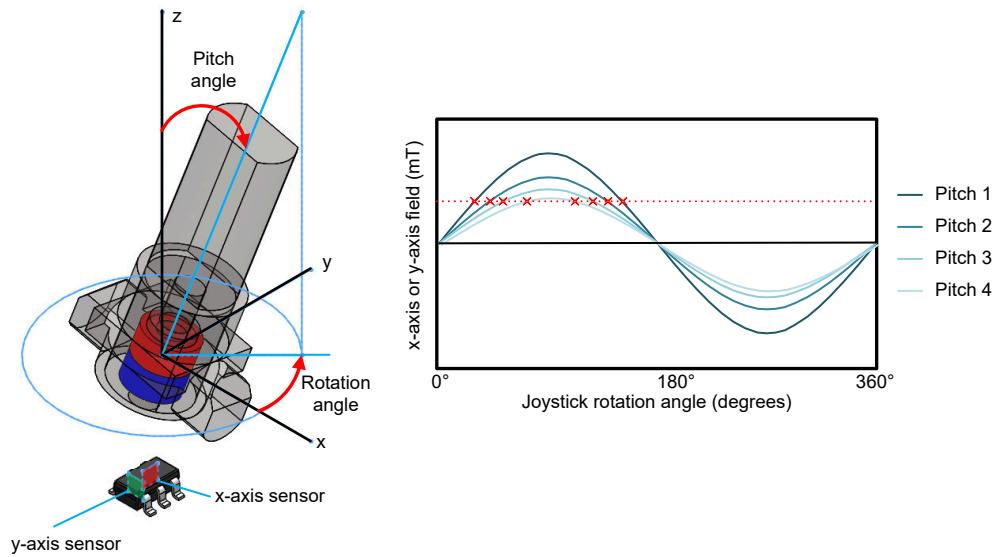


Figure 2-3. Aliasing

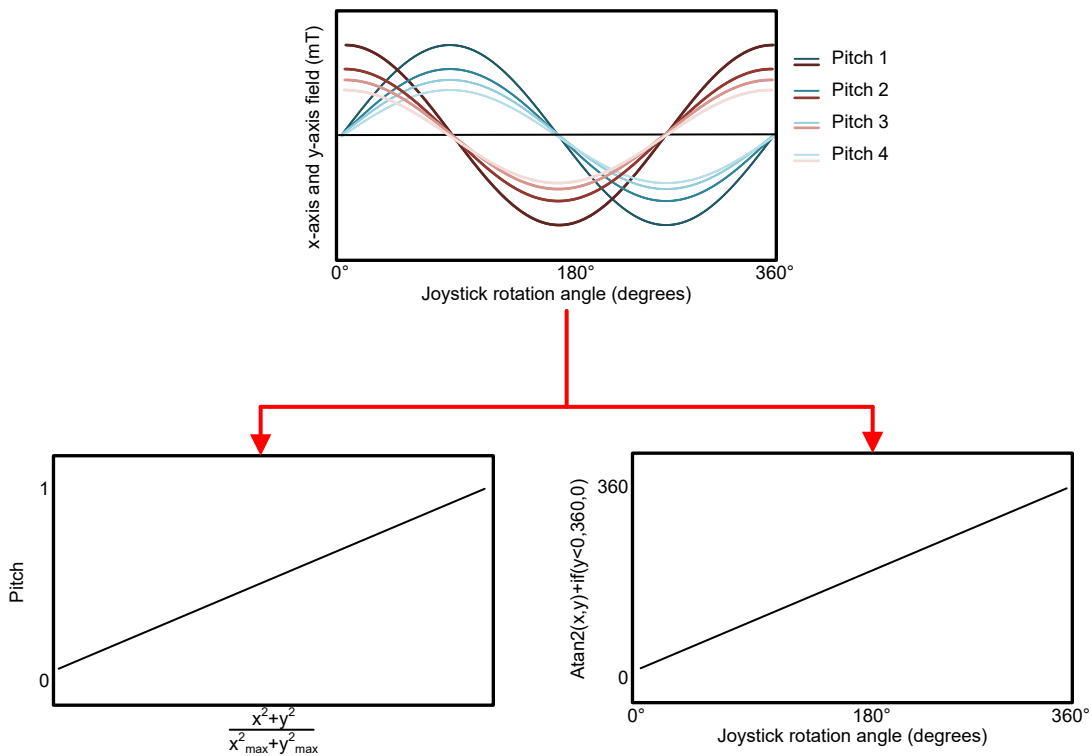
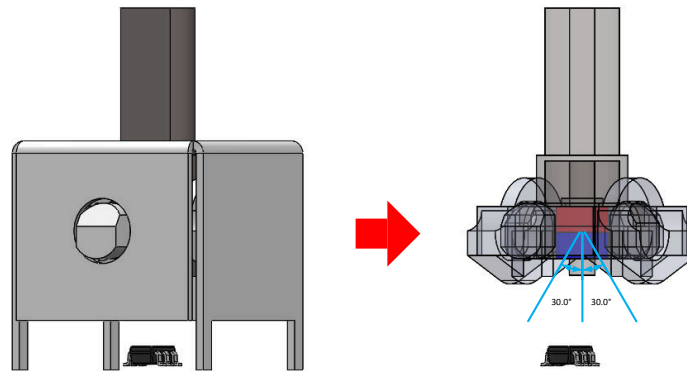
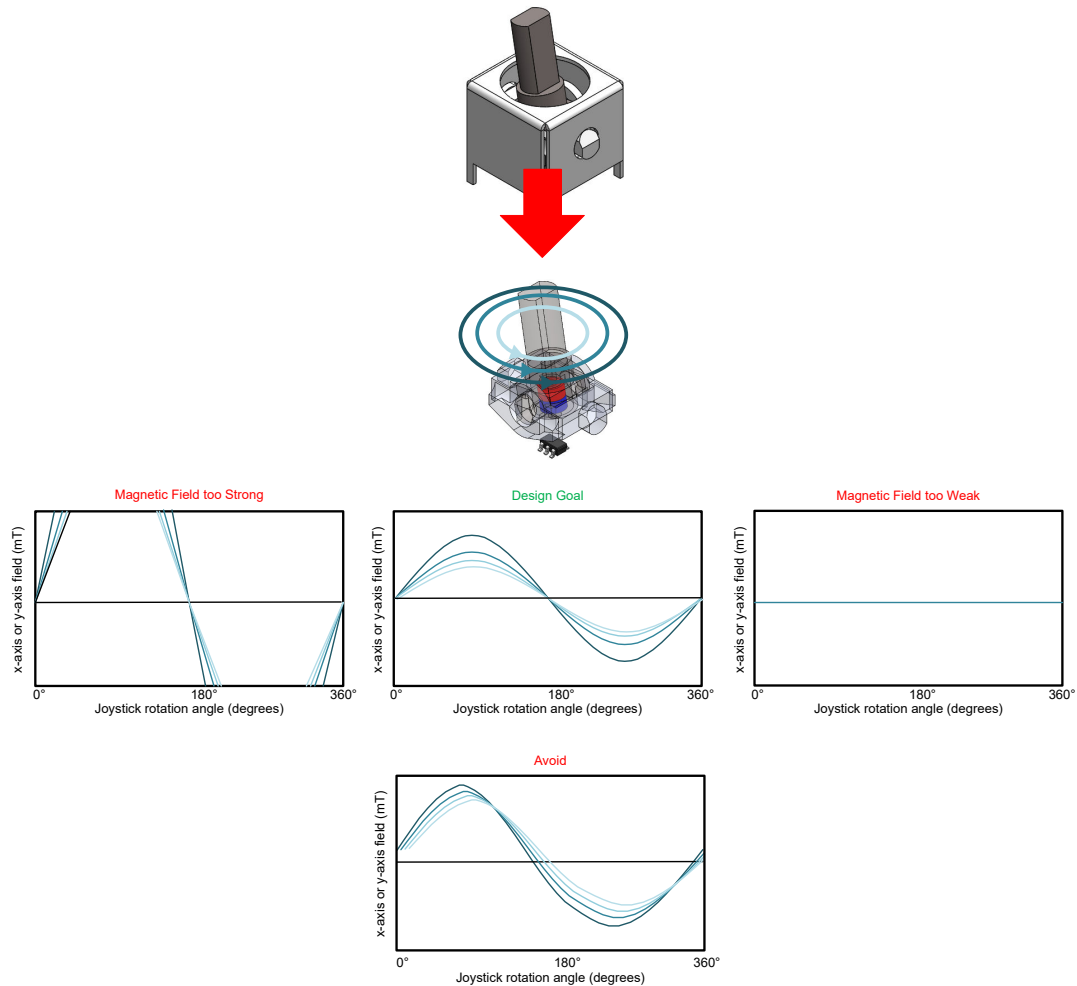


Figure 2-4. 2 Sensor Pitch and Rotation Extraction

Figure 2-5 shows a single device design that utilizes a 3D sensor like the [TMAG5273](#), which has hall elements sensing along the x and y axis, or the [TMAG3001](#) for space constrained applications. For this design, strive to place the device such that you obtain an output similar to Figure 2-6. As the joystick shaft is moved in a circular path for a given pitch, the x-axis and y-axis fields exhibit a sinusoidal behavior relative to the sensor.



**Figure 2-5. 1 Device Design**



**Figure 2-6. 1 Device Example Plots**

Figure 2-7 shows a two device design that utilizes 2 Hall-Elements sensing along the z-axis with output behavior as indicated in Figure 2-8. For the two device design, an analog output device can be used like the [TMAG5253](#) or if there is not an available ADC, a digital design like the [TMAG5273](#) or [TMAG3001](#) can be used.

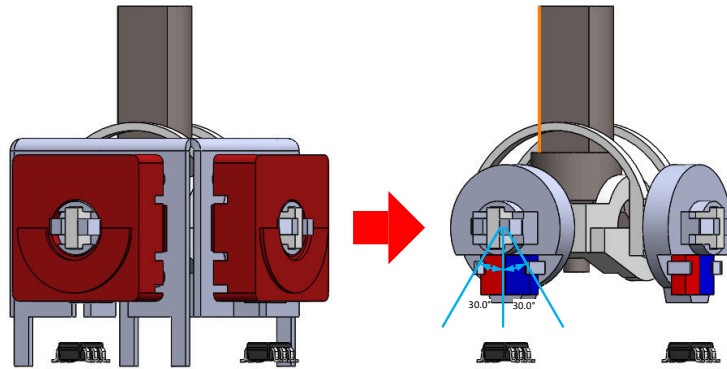


Figure 2-7. 2 Device Design

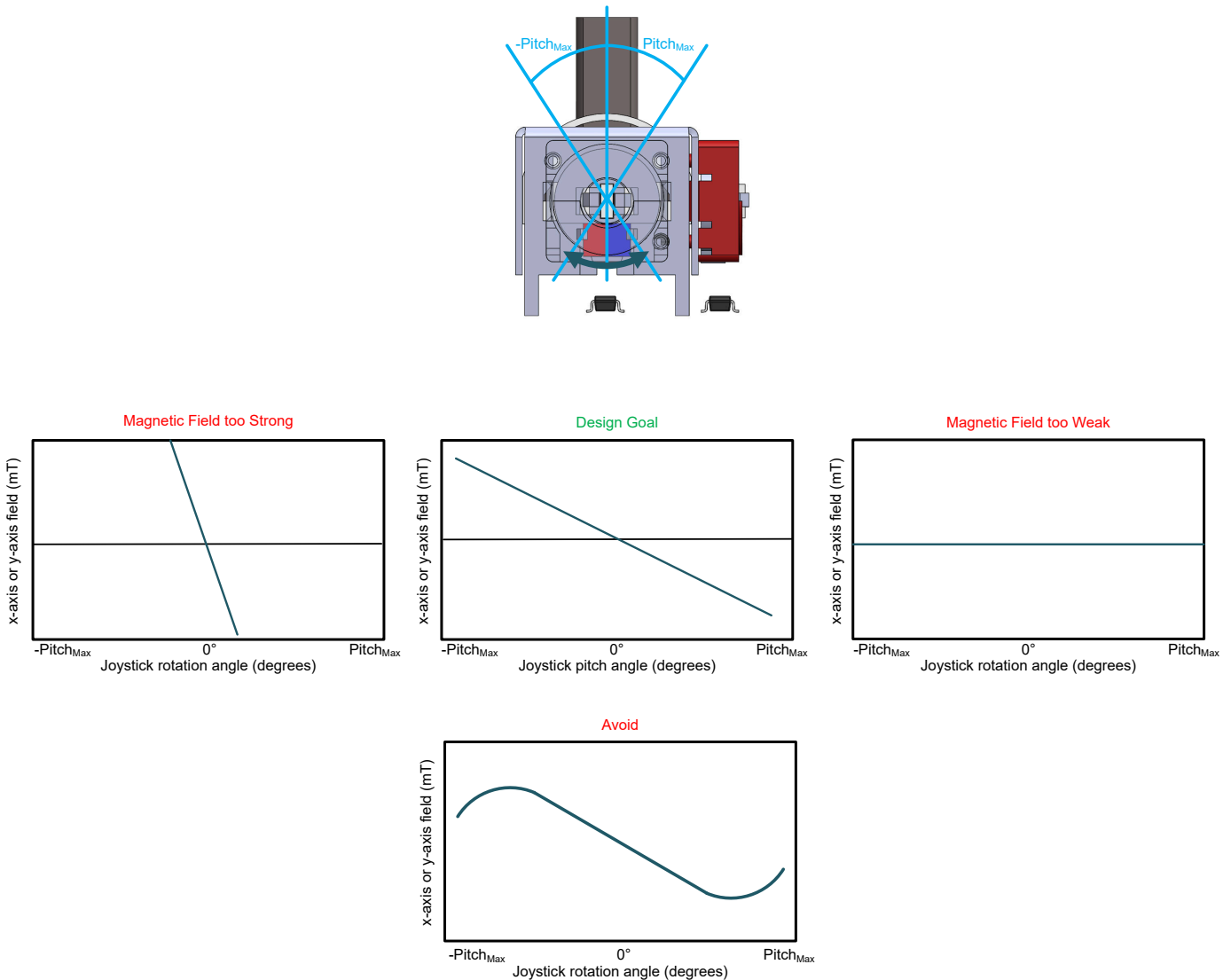
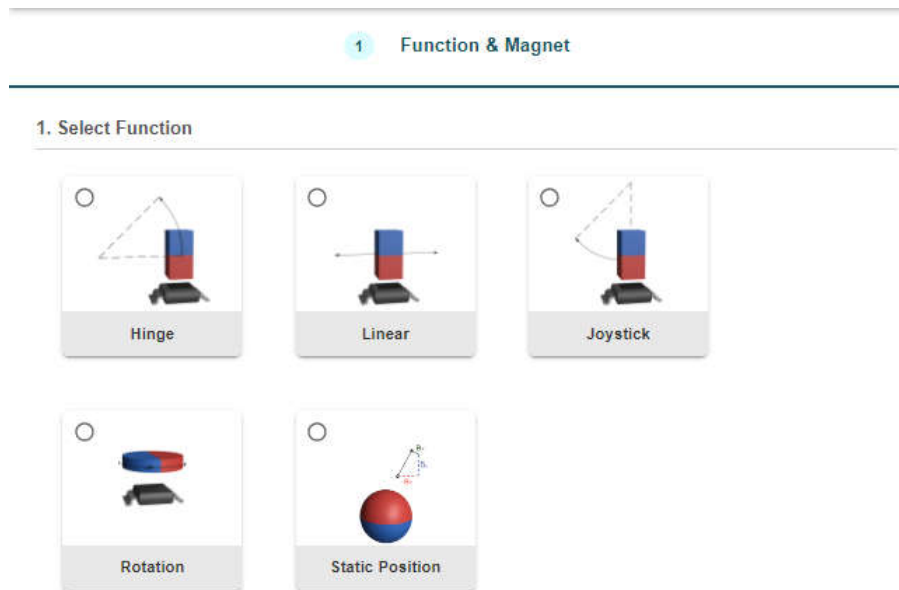


Figure 2-8. 2 Sensor Design Goal

## 2.3 Design Calculations

Having established general expectations of what output is needed for the design, the iterative process of finding the exact placement regions can now be executed. TI offers a [Magnetic Sense Simulator](#) to facilitate this process. This tool has a main menu, where the user can specify the type of magnet movement. The user selection then takes them to a sub-menu with entries to specify magnet placement, sensor placement, range of motion, and device of interest. [Figure 2-9](#) shows the top menu and the Rotation movement sub-menu.



**Figure 2-9. Tool Menus**

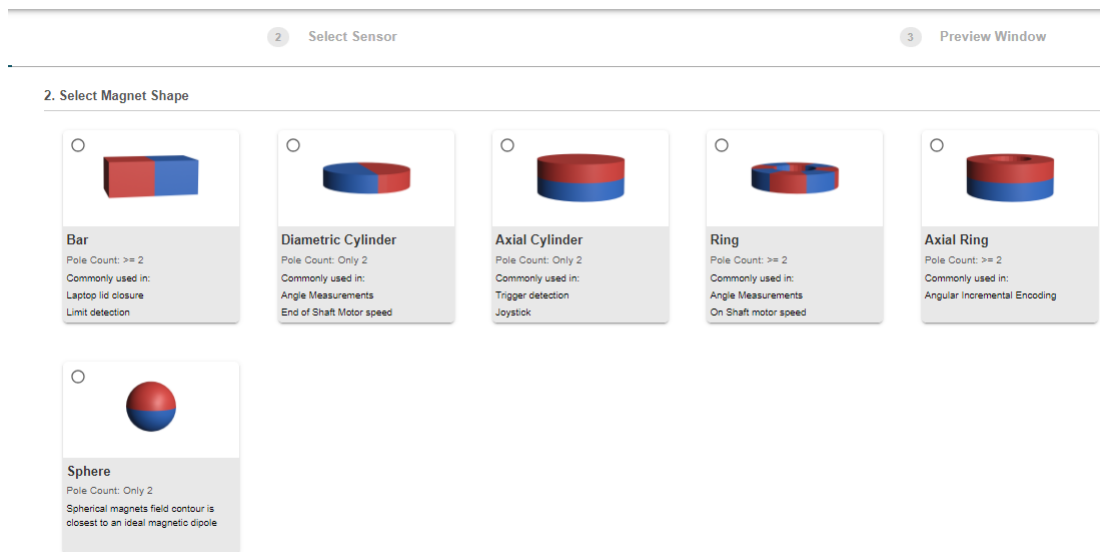


**Figure 2-10. Tool Menus**



For the two-sensor joystick, the inputs required for the desired behavior are shown in Figure 2-11.

Magnet	Sensor	Sim Settings																		
<b>▼ Magnet Specifications</b>																				
Magnet Shape	Bar																			
Poles	2																			
Magnet Material	Sintered Neodymium I...																			
Material Grade	N42																			
<table border="1"> <tr> <td>Select Remanence Value</td> <td>Average Remanence ...</td> </tr> <tr> <td>Remanence (Br)</td> <td>Temperature</td> </tr> <tr> <td>1310 mT at 20°C</td> <td>20 °C</td> </tr> <tr> <td>Temperature Coefficient</td> <td>Coercivity</td> </tr> <tr> <td>-0.12 %/°C</td> <td>11.5 KOe</td> </tr> </table>			Select Remanence Value	Average Remanence ...	Remanence (Br)	Temperature	1310 mT at 20°C	20 °C	Temperature Coefficient	Coercivity	-0.12 %/°C	11.5 KOe								
Select Remanence Value	Average Remanence ...																			
Remanence (Br)	Temperature																			
1310 mT at 20°C	20 °C																			
Temperature Coefficient	Coercivity																			
-0.12 %/°C	11.5 KOe																			
<b>▼ Magnet Geometry</b>																				
Magnet Length - X dim	2.46 mm																			
Magnet Width - Y dim	0.95 mm																			
Magnet Height - Z dim	3.45 mm																			
<b>▼ Magnet Motion</b>																				
<b>Origin Position</b>																				
<table border="1"> <tr> <td colspan="3">Position</td> </tr> <tr> <td>X Axis</td> <td>Y Axis</td> <td>Z Axis</td> </tr> <tr> <td>2.13 mm</td> <td>-1.23 mm</td> <td>0 mm</td> </tr> <tr> <td colspan="3">Angle</td> </tr> <tr> <td>X Axis</td> <td>Y Axis</td> <td>Z Axis</td> </tr> <tr> <td>90 Deg</td> <td>0 Deg</td> <td>-30 Deg</td> </tr> </table>			Position			X Axis	Y Axis	Z Axis	2.13 mm	-1.23 mm	0 mm	Angle			X Axis	Y Axis	Z Axis	90 Deg	0 Deg	-30 Deg
Position																				
X Axis	Y Axis	Z Axis																		
2.13 mm	-1.23 mm	0 mm																		
Angle																				
X Axis	Y Axis	Z Axis																		
90 Deg	0 Deg	-30 Deg																		
<b>Final Position</b>																				
<table border="1"> <tr> <td colspan="2">Position</td> </tr> <tr> <td>Arc Length</td> <td></td> </tr> <tr> <td>60 Deg</td> <td></td> </tr> </table>			Position		Arc Length		60 Deg													
Position																				
Arc Length																				
60 Deg																				

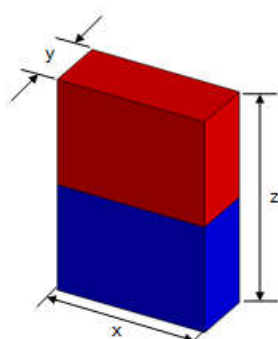
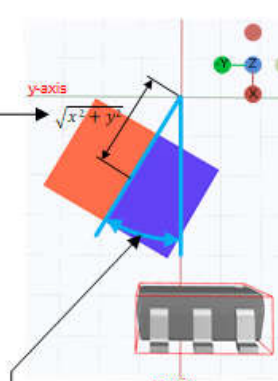
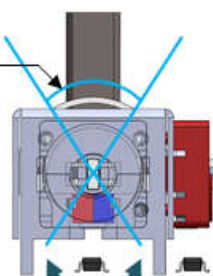




Figure 2-11. 2 Magnet and Sensor Thumbstick Input

Magnet
Sensor
Sim Settings

▼ Sensor Details
⊙

Edit Sensor Selection

Sensor Select      Sensor 1 : TMAG5273 ▼

▼ Sensor Specifications
⊙

Sensor Family		Multi-axis linear & angle po	
Device		TMAG5273	
Part Number		TMAG5273A1QDBVR ▼	
Package	SOT-23	Pin Count	6
Max Vcc	Min Vcc	Applied Vcc	
3.6	V 1.7	V 3.3	V
Max Input	40 mT	Min Input	-40 mT
Input Referred Noise	X: 125 Y: 125 Z: 68 $\mu$ TRMS		
Sensitivity	51.2 LSB/mT		
Sensitivity DirY-X-Z	Quiescent O/P	0	code
Temperature Compensation	0		%C
Averaging	1		Samples

▼ Sensor Position
⊙

Position Properties
⊙

Position

X Axis	Y Axis	Z Axis
6.01 mm	0.4 mm	0.12 mm

Angle

X Axis	Y Axis	Z Axis
0 Deg	-90 Deg	0 Deg

**Figure 2-12. 2 Magnet and Sensor Thumbstick Input**

Plots

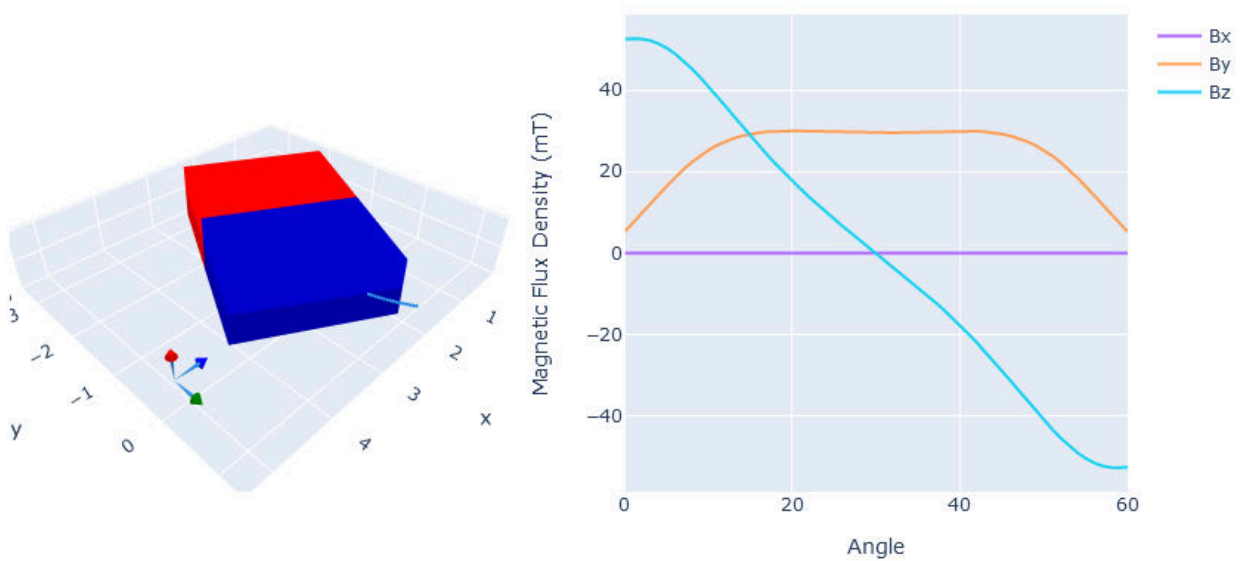


Figure 2-13. Tool Output for 2 Sensor Thumbstick Input

### 2.4 Post Processing

Regardless of whether the joystick is implemented with 1 magnet and 1 sensing device or 2 magnets and 2 sensing devices, some post processing is required to translate measured data into position data relevant to the end user. Postprocessing takes measurements corresponding to the joystick pitching along x-axis and along the y-axis to extrapolate rotation angle and pitch angle.

For the 2 magnet, 2 device design, calibration involves finding the global maximum and minimum values for the z-axis field observed on both sensors. One device's z-field values relate to the joystick movement in the x-direction while the other device's z-field values relate to joystick movement in the y-direction. The bound measurements serve as a reference upon which future measurements can be compared. To find these bound values the user needs to move the joystick around the movement region perimeter as shown in Figure 2-14 and the device sampling rate is significantly faster than the user moving the joystick around the movement region perimeter. This increases spatial resolution in the calibration phase and ensure a higher probability of the ideal global maximum and minimums being detected by the sensor. These values are expected to be found at 0°, 90°, 180°, and 270°, which a user could easily miss by a few degrees if the user simply tried to calibrate by only moving to those visually perceived angles.

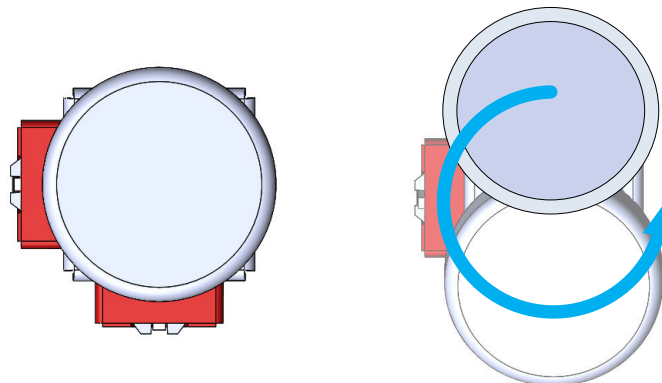


Figure 2-14. Circle Movement for Determining Global Maximums and Minimums

Because an unintended offset between device and sensor in the plane of rotation is expected to have influence on the linearity of the measurement, the default rest position and joystick bound measurements can be determined. This can be measured when the thumbstick is at the resting position. Alternatively, if the resting position is expected to have some tolerance, a calculation of the average position through the previously determined global maximums and minimums can be used.

With the x and y bound values calculated as well as the middle resting position, a rotation value can be calculated. The underlying concept leveraged is stated in [Equation 1](#). However, in this case the all measured x and y values are normalized with respect to the global maximum and minimum values found during calibration like in [Equation 2](#).

$$\text{Angle} = \arctan\left(\frac{y}{x}\right) \quad (1)$$

$$\text{Angle} = \arctan\left(\frac{y_{\text{component}}}{x_{\text{component}}}\right) = \arctan\left(\frac{\frac{Y_{\text{measured}} - Y_{\text{Center}}}{Y_{\text{Bound}} - Y_{\text{Center}}}}{\frac{X_{\text{measured}} - X_{\text{Center}}}{X_{\text{Bound}} - X_{\text{Center}}}}\right) \quad (2)$$

As normalization leads to all x component and y component values ranging between 0 and 1, only angles between 0 and 90° are calculated. Therefore signs need to be assigned to the x\_component and y\_component. How signs are assigned depends on magnet polarity which can vary if there is not consistent assembly. [Figure 2-15](#) shows that there are four different ways the magnets can be installed for the 2 magnet 2 sensor direction. Consequently, a function like in the following pseudo code can be used.

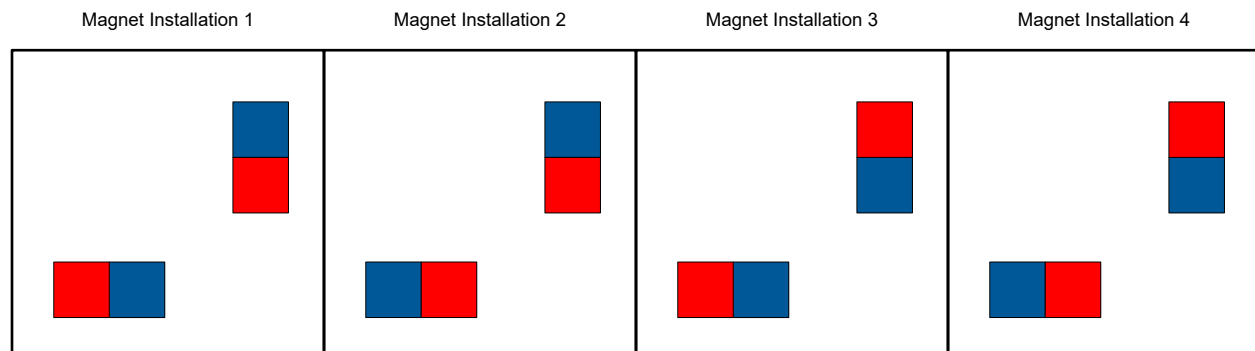


**Figure 2-15. Magnet Installation**

```
float AngleComponent(const float measured, const float Left_Down_Bound, const float Right_Up_Bound,
const float Center)
{
    float angleComponent;
    if(measured > Center)
    {
        if(Left_Down_Bound > Center)
        {
            angleComponent = -(measured-Center)/(Left_Down_Bound-Center);
        }
        else if(Right_Up_Bound > Center)
        {
            angleComponent = (measured-Center)/(Right_Up_Bound-Center);
        }
    }
    else if(measured < Center)
    {
        if(Left_Down_Bound < Center)
        {
            angleComponent = -(measured-Center)/(Left_Down_Bound-Center);
        }
        else if(Right_Up_Bound < Center)
        {
            angleComponent = (measured-Center)/(Right_Up_Bound-Center);
        }
    }
}
```

```
    return angleComponent;
}
```

One pitfall of the arc-tangent function, commonly abbreviated to atan(), is that this function calculates values between -90° and 90°. To get the entire range of angles in a circle, atan2() must be used. However, this function calculates values between -180° and 180°. Therefore, if angles are strictly desired in positive values, a ternary operator can be included in the calculation like in [Equation 3](#).

$$\text{Angle} = \text{atan2}\left(\frac{y\_component}{x\_component}\right) + (y\_component < 0 ? 360 : 0) \tag{3}$$

Joystick pitch can then be extrapolated from the measured data with [Equation 4](#) so long as the movement region bounding pitch angle is known.

$$\text{Angle} = \text{Pitch}_{\max} \times \left(\frac{x^2 + y^2}{x_{\max}^2 + y_{\max}^2}\right) \tag{4}$$

## 2.5 Prototyping and Bench Testing

While simulation can be helpful for the preliminary design and assessing feasibility, prototyping and bench testing is necessary for verifying actual performance. Simulation sometime does not account for all parameters and therefore can not exactly match real world test cases. Bench tests reveal some of the possible discrepancies from designed simulations, thereby exposing subtle neglected influences in the preliminary design phase and as well as offsets that can occur in the manufacturing and assembly process.

For assessing the hardware design, [TMAG5273](#) measurements and joystick movement were captured simultaneously with the setup shown in . In this setup, the phone camera captures a video of the trigger moving while a computer screen captures measurements output in the [TMAG5273EVM GUI](#). Both video files are then synced through an audible impulse. In the phone-captured video, a pointer is attached to the joystick shaft to help visualize joystick angle compared against a protractor centered at the hinge origin. To simplify assessment, movement was restricted by a 3d printed slot to allow only one joystick hinge to rotate at a time.



**Figure 2-16. Thumbstick Hardware Test**

From the [Figure 2-16](#) setup the measurements in [Figure 2-17](#) were collected.

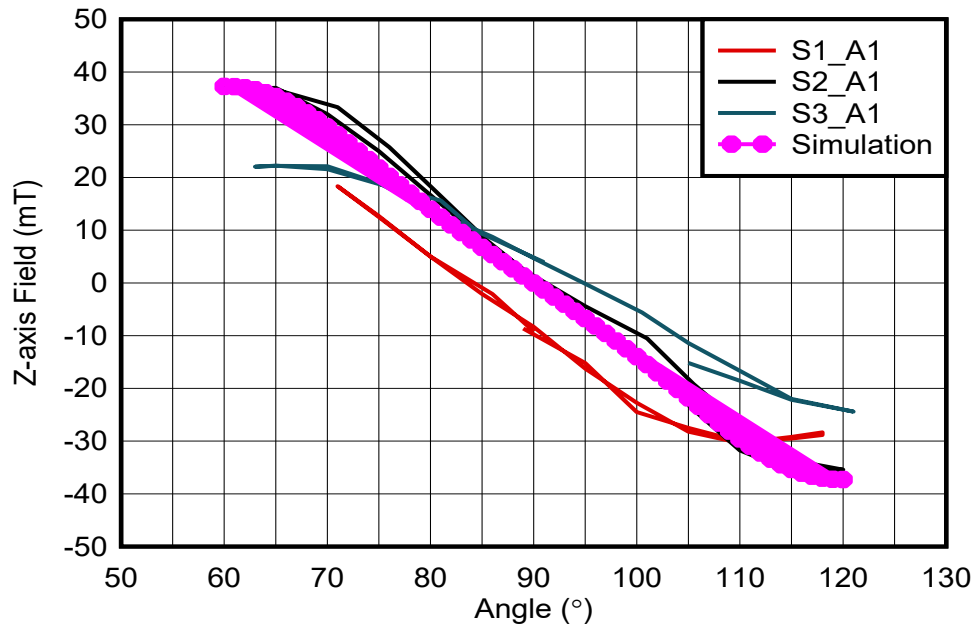


**Figure 2-17. Final Hardware Test Data**

For assessing the software processing algorithm, a separate test setup was used. A 3D printer was outfitted with a special attachment to control the movement of the joystick as shown in [Figure 2-18](#) and custom g-code was generated to direct the 3D printer how to move. From this test setup, the [Figure 2-19](#) data in was collected.

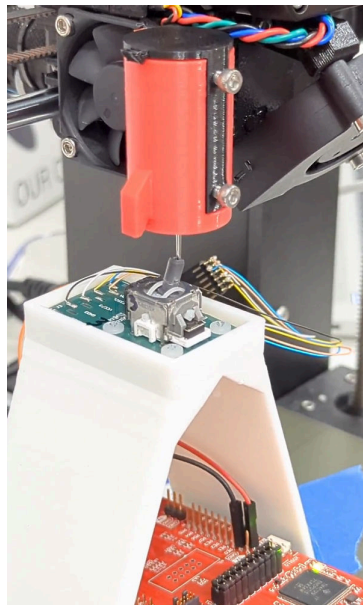


**Figure 2-18. Software Test Setup**

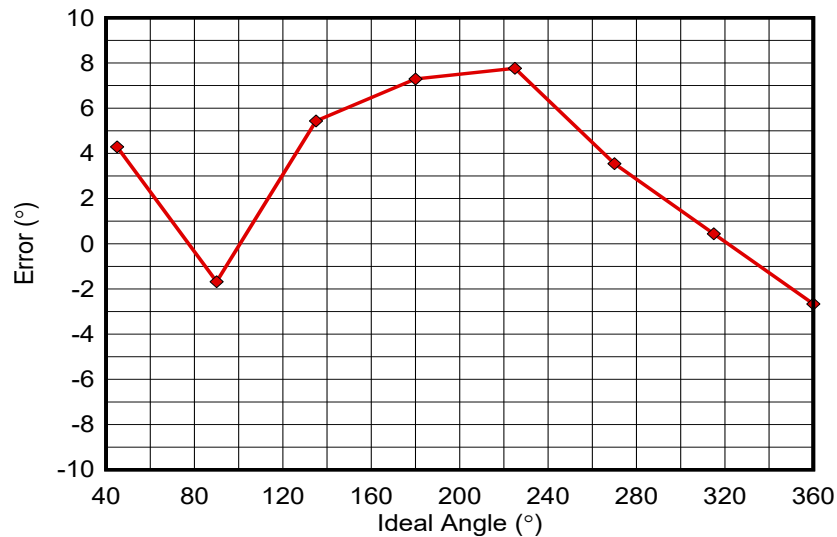


**Figure 2-19. Final Software Data**

The data presented in this section correspond to the final sets acquired after various iterations of debugging the test setup and adjusting for some assembly flaws. The prior collected data revealed potential issues that were not fully accounted for in the preliminary design calculations.

## 2.6 Error Sources

There are several possible sources of error, many of which correspond to fabrication and assembly. In the process of evaluating on the bench such error sources are easier to identify, thereby making bench testing a good and necessary practice to embrace before proceeding to mass production. The following list shows all possible error sources identified for this particular design including the ones accounted for in the preliminary design:

- Fabrication Limitation and mechanical tolerance
- Operating outside of the linear region
- Device offsets
- Roll, Yaw, and Pitch
- Magnet Variation
- Device Variation and Temperature Drift
- External Fields
- Nearby Material Influence
- Bench Setup Error
- Supply Tolerance
- Measurement precision

The most notable errors for the 2-magnet-2-sensor thumbstick prototyped in this application note resulted in data curve that exhibited hysteresis. One significant error source was the mechanical hysteresis stemming from material selection and fabrication tolerance, while the other was the magnetic properties of the nearby materials. These errors were quite significant when not accounted for and do affect the post processing calibration and calculation results. Prior to addressing the mechanical hysteresis, the hardware data in [Figure 2-20](#) exhibited noticeable hysteresis and resulted in the large error observed in [Figure 2-21](#). Other notable errors include offset and fulcrum slippage.

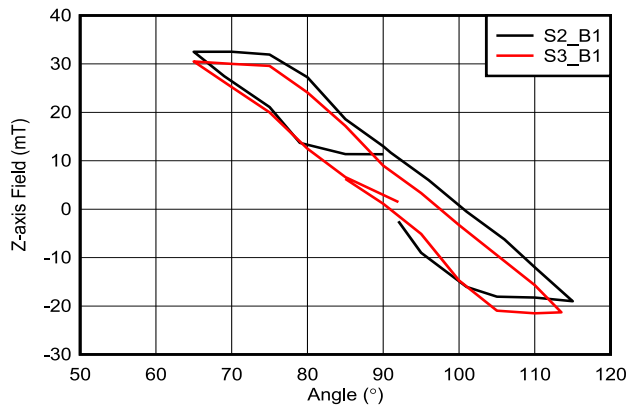


**Figure 2-20. Preliminary Hardware Test Error Before Debug and Adjustment**

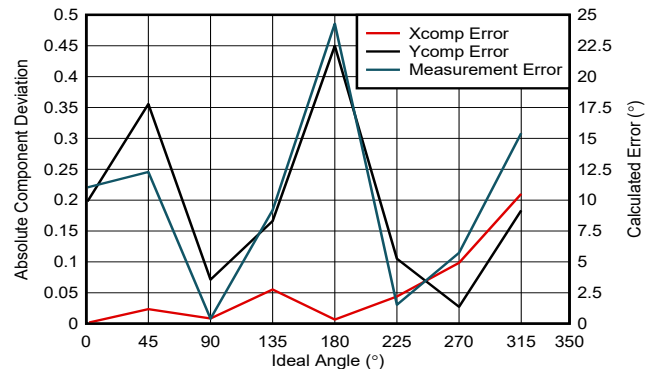


**Figure 2-21. Preliminary Software Test Error Before Debug and Adjustment**

### 2.6.1 Mechanical Hysteresis

Friction coupled with the modulus of elasticity were found to contribute mechanical hysteresis for the 2 sensor 2 magnet thumbstick tested in this application note. Consequently, the stick component appeared to be moving while the magnet was not, resulting in movement similar to what is shown in Figure 2-22 where the left thumbstick is in the default resting position with the magnet centered as expected while for the right thumbstick the stick is tilted to the left but the magnet has not moved by any discernible amount. Part tolerances and materials with a low coefficient of friction are important for minimizing this error.

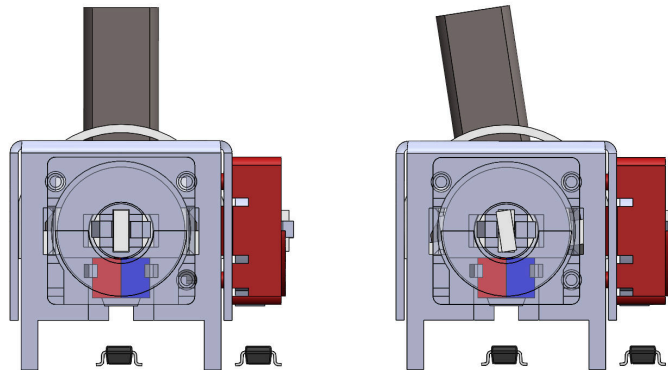


**Figure 2-22. Mechanical Hysteresis**



### 2.6.2 Nearby Material Influence

As mentioned in the list of errors, nearby materials can influence measurements. Highly permeable materials like iron, cobalt, nickel, and steel can not only redirect field through the path of least reluctance, but can also resist demagnetization associated with magnet movement. In an ANSYS transient simulation we are able to observe that if the magnet and sensor are placed close to a structure made out of a permeable material like nickel, hysteresis can be observed when the direction of movement is reversed as indicated in [Figure 2-23](#).

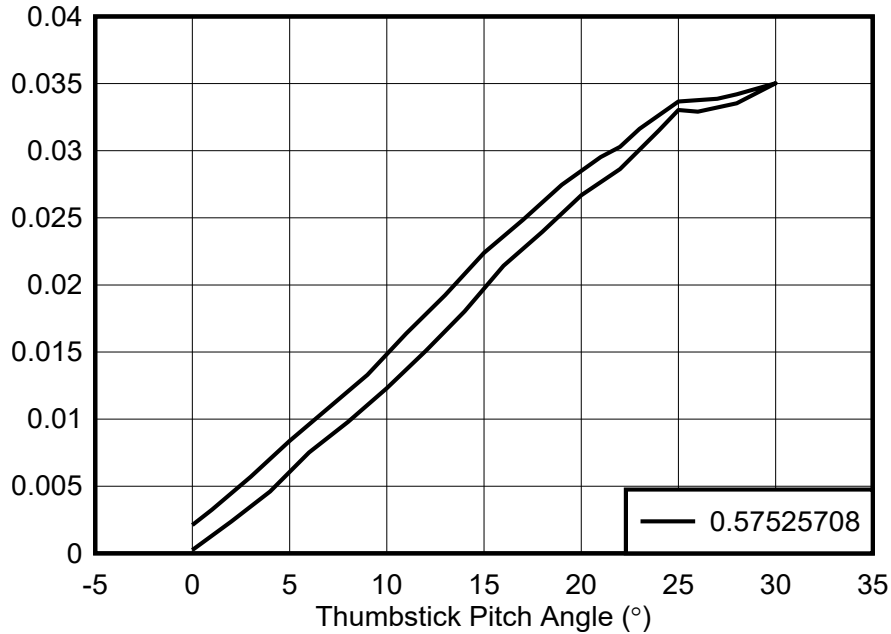


**Figure 2-23. Magnetic Hysteresis**

### 2.6.3 Fulcrum Slippage

In excellent choice scenario simulated in the design section, the fulcrum is fixed and unmoving. However, depending on the tolerances of the joystick assembly, there can be some room for fulcrum point to slip. This can change the path of the magnet as illustrated in [Figure 2-24](#).

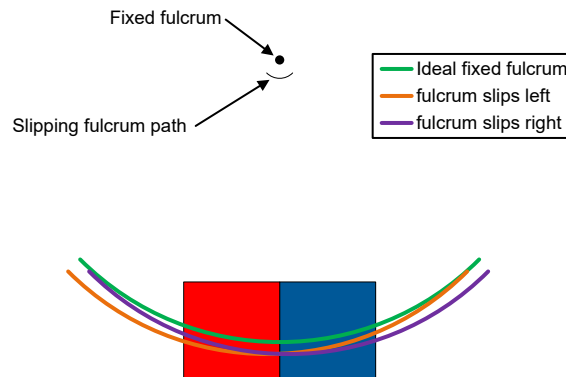


**Figure 2-24. Fulcrum Slip**

### 2.6.4 Offset

Offset corresponds to the magnet not being centered properly over the device sensing element, indicated by the blue box in Figure 2-25. Offset along the y-axis as defined in Figure 2-25, is not as bad as offset along the x-axis or z-axis. Increasing the offset along the z-axis decreases the field strength measure by the device. Whereas offset along the x-axis shifts the field characteristic and decreases the usable linear range.

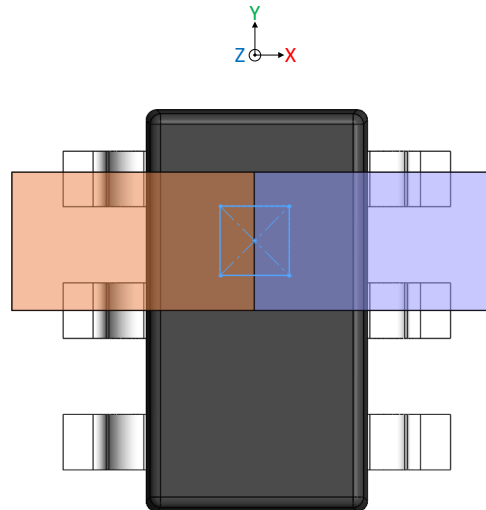


**Figure 2-25. Magnet Rotating in Device zx Plane**

### 3 Lever Design

Lever controls are functionally similar to the joystick discussed previously, but typically have motion constrained along a single axis of rotation at a time.

#### 3.1 Establishing a Form Factor

For this application, it is functionally possible for either the sensor or the magnet to be located on the pivoting part of the lever, but again, it is much more convenient for the magnet to move while sensor location remains fixed.

##### 3.1.1 Choosing Mechanical Implementation

There are two typical alignments which can be implemented in a straight-forward manner. Either the sensor PCB is located co-planar to the plane of rotation for the pivoting magnet, or the PCB would be installed with the sensor parallel to the plane of rotation. Both alignments are shown in [Common Lever Alignments](#). While it is possible to orient the PCB freely when using a 3D Hall-effect sensor, this convention will be used for simplicity.

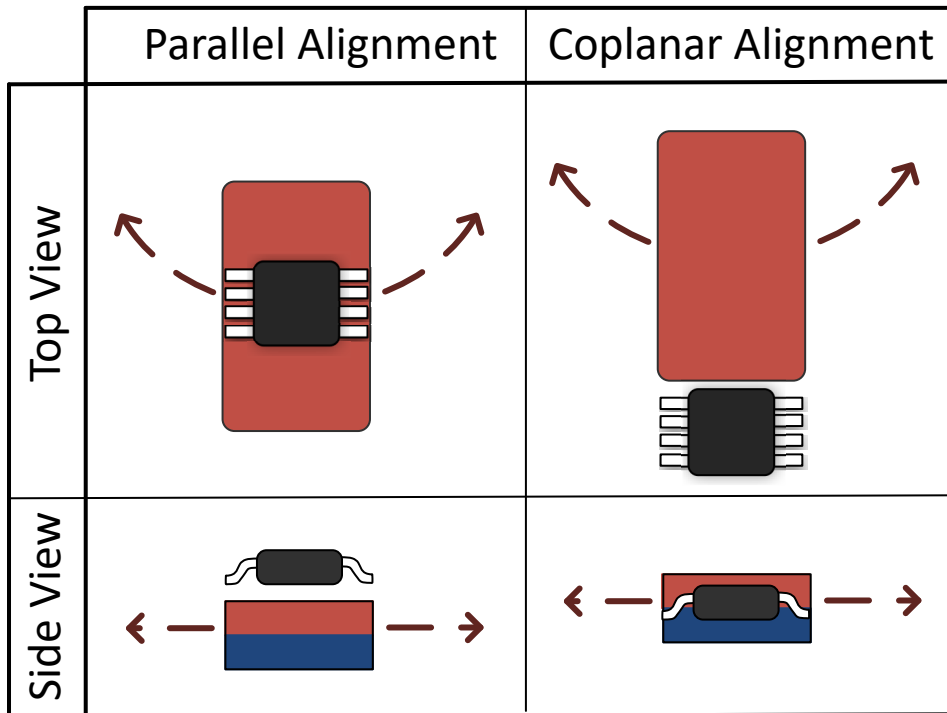


**Figure 3-1. Common Lever Alignments**

In many instances co-planar installation will require a larger system footprint. For this reason, a parallel installation will be explored in the following example to maintain a minimal design size within a turn indicator stalk.

Another consideration to account for is the range of travel for the lever. Common automobile applications are shown in [Lever Motion Types](#). Omni-directional lever, similar to what might be experienced implementing a [e-Shifter Design](#) using a traditional lever is only able to rotate about a single axis. [Steering Column Levers](#), such as a turn indicator or windshield wiper control, are typically able to tilt bi-directionally supporting two axes of rotation.

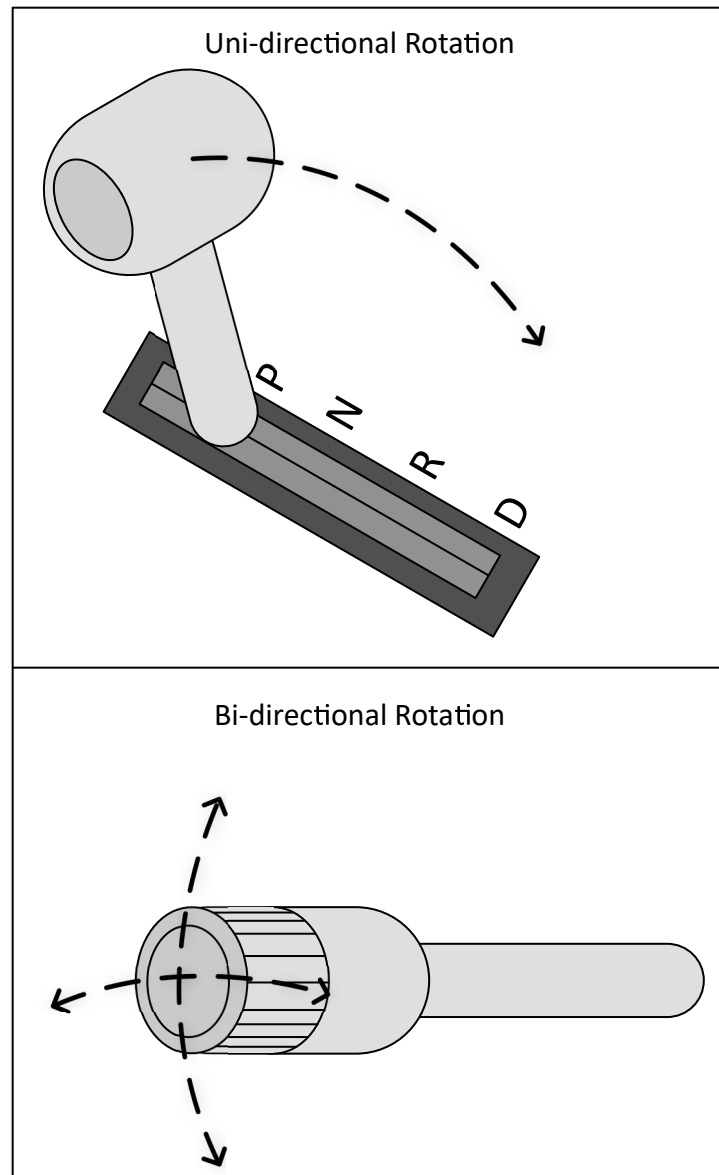


**Figure 3-2. Lever Motion Types**

While not in use, the turn indicator resides at a center position, but at any time the lever can be pulled toward the driver to toggle the flash-to-pass function. This flash-to-pass function will temporarily enable the high beam headlights until the driver releases the control. This example will demonstrate the retro-fit of a production turn-indicator module using a single Hall-effect sensor shown in [Turn Indicator Stalk](#).

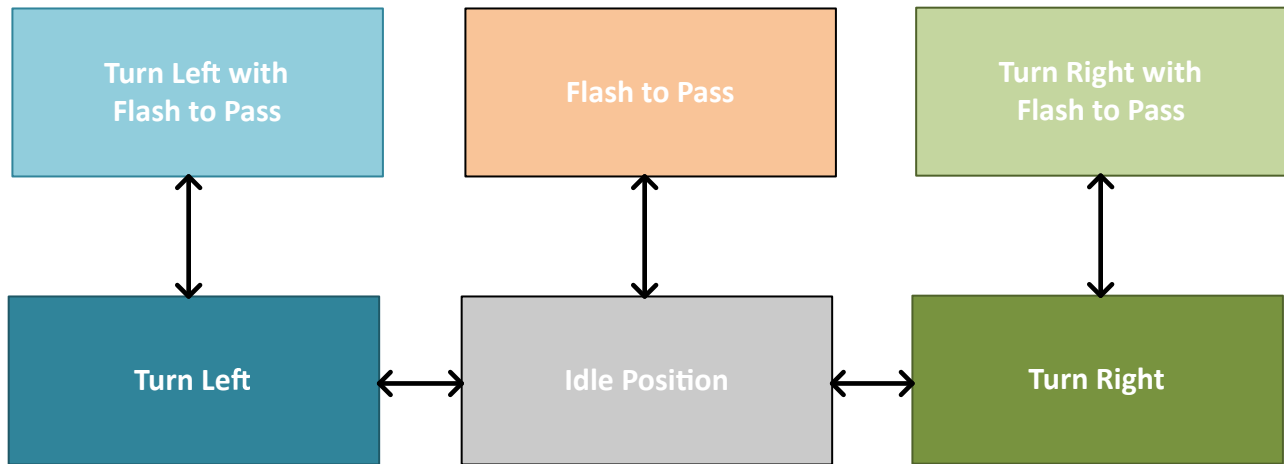


**Figure 3-3. Turn-Indicator Functional States**



**Figure 3-4. Turn Indicator Stalk**

### 3.2 Magnet Sensor Placement

As discussed in [Section 2](#), it is important to position the magnet in such a way to utilize as much of the linear input range of the sensor without saturating the inputs. Sweeping the magnet position near a 3D Hall-effect sensor will produce a behavior similar to what is shown in [Example Lever Input Field](#). It is typical that a component of the field vector will have a somewhat triangular or S shape, while the other two components will have a bell shape. The magnitude of each vector component will depend on alignment.

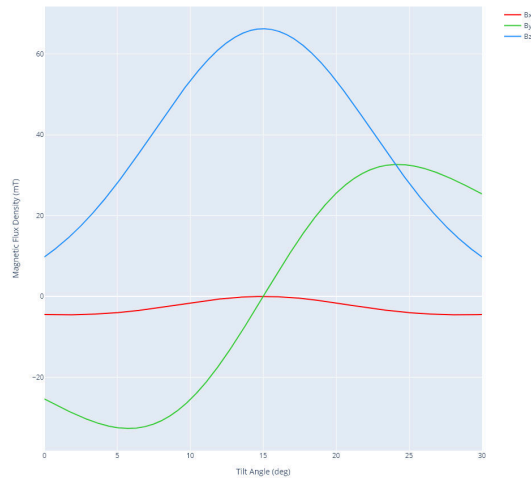


**Figure 3-5. Example Lever Input Field**

To maximize the input range for a control such as the turn indicator stalk, the mid-point position for the magnet must be centered above the magnet. For this case, where the magnet location is not placed on the rotating fulcrum of the control, it becomes necessary to use a single multi-axis sensing device similar to what was presented in [Section 2](#), using one of the configurations presented in [Figure 3-1](#)

A first reason for this requirement can be observed in [Example Lever Input Field](#). As the lever pivots to either +15 or -15 degrees relative to the idle position, we see the challenge that aliasing can create when observing  $B_z$ . Even if using the  $B_y$  component, there are positions above +/- 10 degrees from center where the input field can be mapped to a second location.

Additionally, if only observing a single axis, the lever pull for flash-to-pass will increase the distance between the magnet and sensor. If only using a single axis of sensitivity, this motion can also become ambiguous and can be confused with a left or right turn setting.

### 3.3 Design Calculations

To properly place the sensor within the existing steering column control module, one must understand the expected magnetic field that can result from the lever motion

The best location for the magnet to be installed in this test case is near the end of stalk shaft where an exposed section of the lever is exposed. The opening is approximately 12 mm × 6 mm, and a magnet of this size is easily installed as shown in [Turn Indicator Magnet Location](#). [TMAG5170-Q1](#) was selected as a sensor to fit into the design using the [TMAG5170UEVM](#) connected to the [TI Sensor Control Board](#).

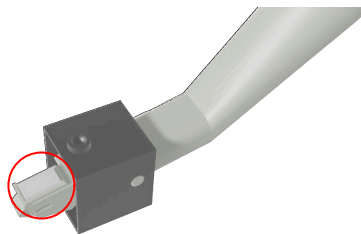


**Figure 3-6. Turn Indicator Magnet Location**

Measurements of the available mounting locations for both the magnet and [TMAG5170-Q1](#) sensor were taken and used to simulate the expected input to the 3D Hall-effect sensor using the [TI-Magnetic-Sense-Simulator](#).

First, with the turn-indicator lever traveling through the standard turn positions, the simulated input field components are shown in [Simulated Turn Indicator Input Field](#), and the alignment between the sensing element and the magnet travel are depicted in [Turn Indicator Magnet Motion](#).

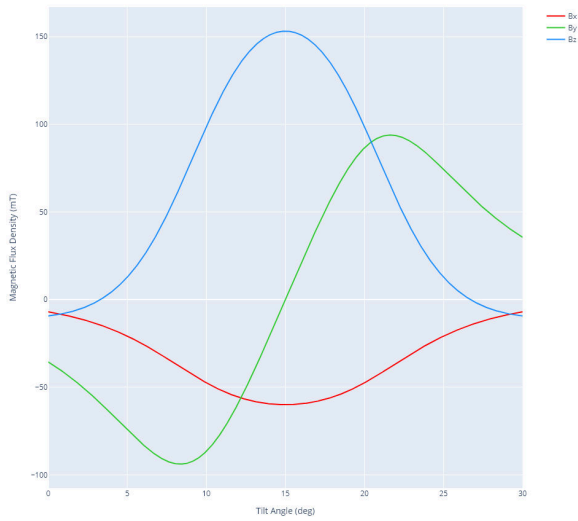


**Figure 3-7. Simulated Turn Indicator Input Field**

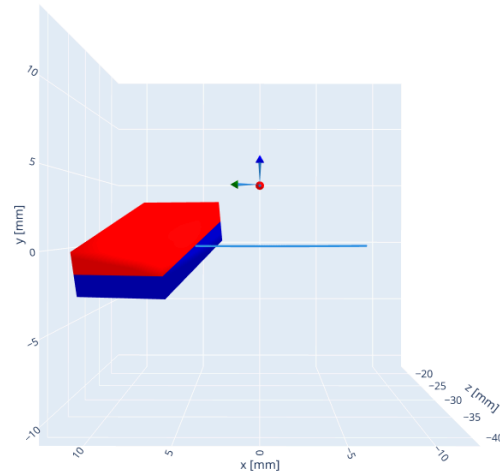


**Figure 3-8. Turn Indicator Magnet Motion**

Simulating the magnet rotation about the Z axis (blue) shows that a spacing of 4.3 mm provides a  $B_z$  component which exceeds 150 mT, requiring that the input magnetic range for *TMAG5170A2-Q1* be set to +/-300 mT range. With this range set, a secondary simulation for the flash-to-pass lever pull were conducted to observe the minimal expected input fields when the range to the sensor is increased by the user.

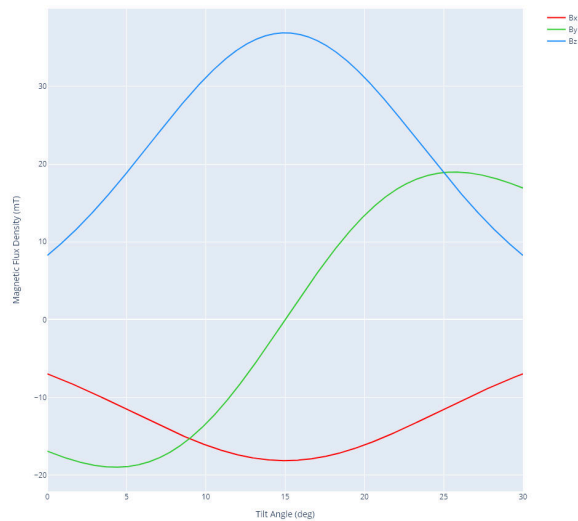


**Figure 3-9. Simulated Flash-to-Pass Input Field**

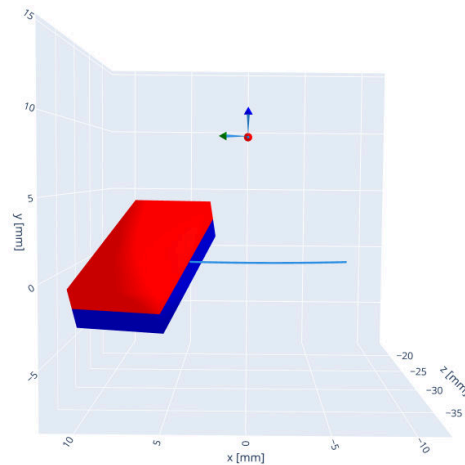


**Figure 3-10. Flash-to-Pass Magnet Motion**

As a result of the additional tilt during flash-to-pass, there is a clear reduction in magnitude across all three magnetic field vector components, but there remains a large enough input signal that SNR is not a challenge.

### 3.4 Prototyping and Bench Testing

With a high degree of confidence in the output format the lever design was assembled and installed into the existing automotive steering column control module.

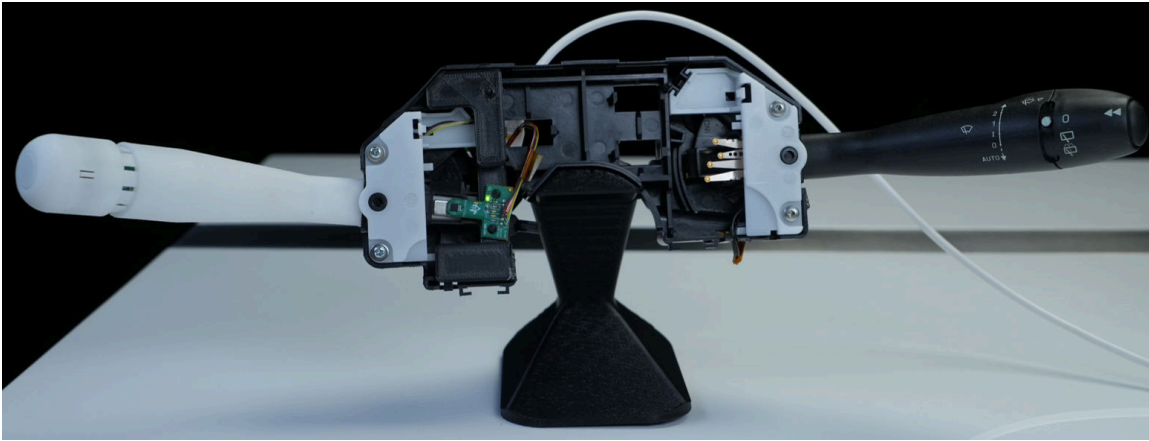


**Figure 3-11. Automobile Turn Indicator Demo**

Sensor data for all three axes was then streamed continually while the indicator stalk was moved through all operating positions. When plotting the collected X, Y, and Z component data in [XYZ B-field Data](#), three very distinct travel arcs are revealed.

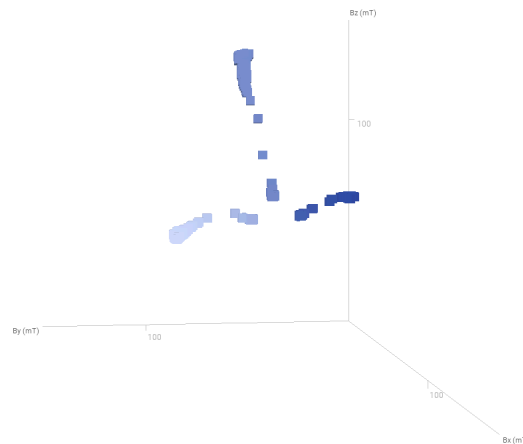


**Figure 3-12. XYZ B-field Data**

The raw X, Y, and Z component data can be used sufficiently well to create a look-up table which can be used to define each of the six operation positions. However, performing vector angle calculations from these results provides an even clearer decision tree. These vector angle calculations provide a more spherical reference which is useful in joystick and lever applications where multiple axes of data are available. These vector angle calculations are referred to as Alpha( $\alpha$ ) and Beta( $\beta$ ), and when joined with a total vector magnitude are descriptive of the total field vector.

$$\alpha = \operatorname{atan}\left(\frac{\sqrt{B_z^2 + B_x^2}}{B_y}\right) \quad (5)$$

$$\beta = \operatorname{atan}\left(\frac{\sqrt{B_z^2 + B_y^2}}{B_x}\right) \quad (6)$$

$$\text{magnitude} = \sqrt{B_x^2 + B_y^2 + B_z^2} \quad (7)$$



To better understand Equation 5 through Equation 7, consider the vector diagrams in Alpha and Beta Angle Vector Diagrams which use an identical source vector to demonstrate the each angle.

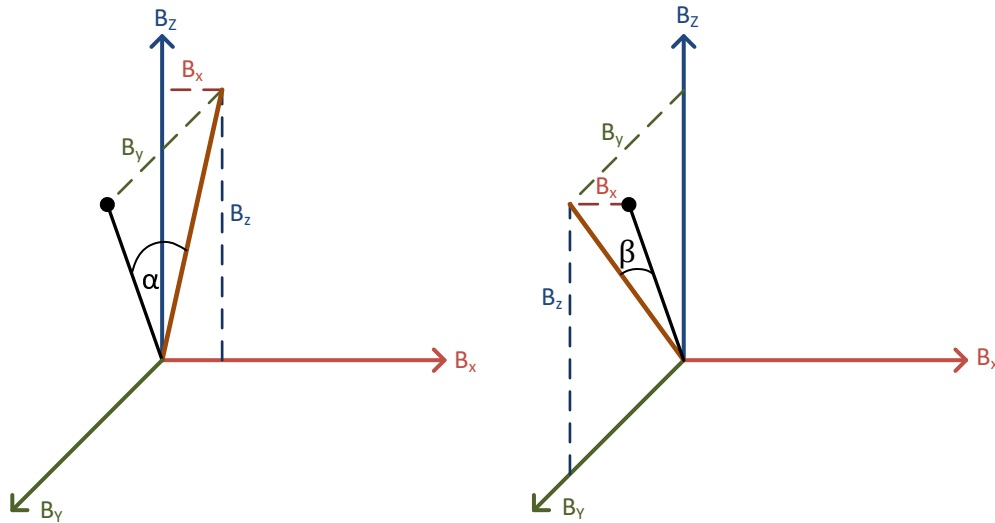


Figure 3-13. Alpha and Beta Angle Vector Diagrams

Applying Equation 5 through Equation 7 to the captured data in XYZ B-field Data, linear changes in angle are easily identified.

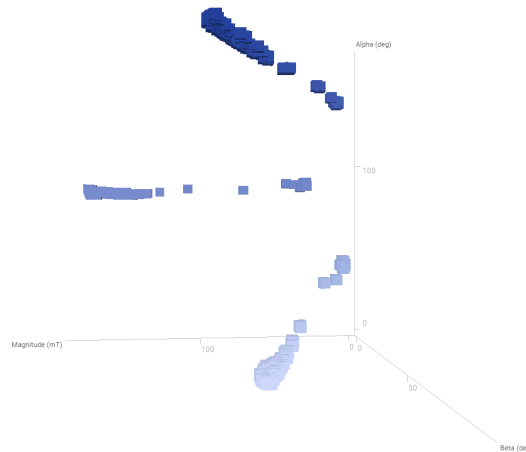


Figure 3-14. Calculated Alpha-Beta Data

After plotting the Alpha and Beta angles against the vector magnitude, it is clear that the Alpha angle result from Equation 5 defines three separate regions for each of the turn indicator positions. The vector magnitude from Equation 7 can be used to easily define the lever pull. Additionally, there is now a linear response to the lever pull action which can be used to indicate how far the lever has been pulled. If desired, Alpha and Beta together can also be used to define many more tilt angles for the indicator stalk.

Example code in TMAG5170-CODE-EXAMPLE and TMAG5x73-CODE-EXMAPLE both provide reference for how to implement these calculations.

### 3.5 Error Sources

Checking the data plots in [Figure 3-12](#) or [Figure 3-14](#) do show some scattering and uncertainty of absolute position. This variation occurs due to looseness of the mechanical tolerances of the assembly. The sensor is sensitive enough to capture the minor variations in magnetic position, and the control was intentionally wiggled through mechanical tolerances of each position to clearly define the limits for operating states.

Aside from this, input referred noise and sensitivity error are the key factors to consider when determining measurement error. Input referred noise produces random variation on the output signal which influences the final angle calculations. Averaging consecutive measurements can reduce this error source. In effect the RMS noise value is reduced by a ratio of the square root of the number of samples.

Sensitivity error is the result of gain variation in the device signal chain and can result in amplitude variations between axes and between devices. The significance of this error on angle measurements tends to vary based on the mismatch between individual axes.

Additionally, one must consider temperature and lifetime drift of the sensor. This can cause minor changes to offset and sensitivity. The significance of any drift can impact the Alpha and Beta angle calculations and result in some small variance to the defined positions of the lever. Applying temperature compensation internal to the sensor greatly reduces any impact due to temperature variations.

For reference, please consider the following 3D Hall-effect sensors and their data sheets electrical table for a complete summary of performance.

**Table 3-1. 3D Hall-Effect Sensors**

Device	Description
<a href="#">TMAG5170</a>	Commercial grade 3D linear Hall-effect sensor with SPI and integrated CORDIC at 1/4 degree resolution.
<a href="#">TMAG5170-Q1</a>	Automotive grade 3D linear Hall-effect sensor with SPI and integrated CORDIC at 1/4 degree resolution
<a href="#">TMAG5170D-Q1</a>	Dual-die automotive grade 3D linear Hall-effect sensors with SPI and integrated CORDIC at 1/4 degree resolution
<a href="#">TMAG5173-Q1</a>	Automotive grade 3D linear Hall-effect sensor with I2C and integrated CORDIC at 1/16 degree resolution
<a href="#">TMAG5273</a>	Commercial grade 3D linear Hall-effect sensor with I2C and integrated CORDIC at 1/4 degree resolution
<a href="#">TMAG3001</a>	Commercial grade 3D linear Hall-effect sensor with I2C integrated CORDIC at 1/16 degree resolution and wake up detection

## 4 Summary

This application note demonstrated that Hall effect sensors can be used in joysticks and levers. The design flow for each example was presented starting with deciding the general mechanical form and the possible magnetic implementation. Subsequently, design calculations were executed through the [TI-Magnetic-Sense-Simulator](#) developed by TI. This tool provided an initial look at high level feasibility for the magnetic position sensing implementation chosen for the joystick or lever. After tackling the hardware design, software algorithms were presented on how measurements from the Hall-effect sensors can be translated into angle values that are more perceptually relate-able to the end user.

Following the post processing algorithms, discussions on prototyping and bench testing were divulged. The bench testing served to substantiate the idea that Hall-effect sensors can be used in joysticks and levers, and are not just hypothetical conjecture supported only by simulation. These bench tests though did reveal that there can be deviation from the simulation results, and is instrumental in finding errors not accounted for in the early stages of design. Consequently, the notable errors for the designs in this application note were presented. With the design flow presented in this document, the reader has the details to quickly mimic, iterate, and possibly improve upon the designs presented.

## 5 References

1. Texas Instruments, [TMAG5273 Low-Power Linear 3D Hall-Effect Sensor With I2C Interface](#), data sheet.
2. Texas Instruments, [Enhanced Proximity tool](#).
3. Texas Instruments, [TMAG5170-CODE-EXAMPLE](#).
4. Texas Instruments, [TMAG5x73-CODE-EXMAPLE](#).
5. Texas Instruments, [e-Shifter Design](#).
6. Texas Instruments, [Steering Column Levers](#).
7. Texas Instruments, [TMAG5170UEVM](#).
8. Texas Instruments, [TI Sensor Control Board](#).
9. Texas Instruments, [TI-Magnetic-Sense-Simulator](#).
10. Texas Instruments, [TMAG5170A2-Q1](#).

## 6 Revision History

<b>Changes from Revision * (June 2023) to Revision A (December 2023)</b>	<b>Page</b>
• Updated the numbering format for tables, figures, and cross-references throughout the document.....	<a href="#">1</a>
• Added <i>TMAG3001</i> throughout the document.....	<a href="#">1</a>

---

## IMPORTANT NOTICE AND DISCLAIMER

TI PROVIDES TECHNICAL AND RELIABILITY DATA (INCLUDING DATA SHEETS), DESIGN RESOURCES (INCLUDING REFERENCE DESIGNS), APPLICATION OR OTHER DESIGN ADVICE, WEB TOOLS, SAFETY INFORMATION, AND OTHER RESOURCES "AS IS" AND WITH ALL FAULTS, AND DISCLAIMS ALL WARRANTIES, EXPRESS AND IMPLIED, INCLUDING WITHOUT LIMITATION ANY IMPLIED WARRANTIES OF MERCHANTABILITY, FITNESS FOR A PARTICULAR PURPOSE OR NON-INFRINGEMENT OF THIRD PARTY INTELLECTUAL PROPERTY RIGHTS.

These resources are intended for skilled developers designing with TI products. You are solely responsible for (1) selecting the appropriate TI products for your application, (2) designing, validating and testing your application, and (3) ensuring your application meets applicable standards, and any other safety, security, regulatory or other requirements.

These resources are subject to change without notice. TI grants you permission to use these resources only for development of an application that uses the TI products described in the resource. Other reproduction and display of these resources is prohibited. No license is granted to any other TI intellectual property right or to any third party intellectual property right. TI disclaims responsibility for, and you will fully indemnify TI and its representatives against, any claims, damages, costs, losses, and liabilities arising out of your use of these resources.

TI's products are provided subject to [TI's Terms of Sale](#) or other applicable terms available either on [ti.com](https://www.ti.com) or provided in conjunction with such TI products. TI's provision of these resources does not expand or otherwise alter TI's applicable warranties or warranty disclaimers for TI products.

TI objects to and rejects any additional or different terms you may have proposed.

Mailing Address: Texas Instruments, Post Office Box 655303, Dallas, Texas 75265  
Copyright © 2023, Texas Instruments Incorporated